

Diffusion-aided Task-oriented Semantic Communications with Model Inversion Attack

Xuesong Wang[✉], Mo Li[✉], Xingyan Shi[✉], Zhaoqian Liu[✉], and Shenghao Yang[✉], *Member, IEEE*

Abstract—Semantic communication enhances transmission efficiency by conveying semantic information rather than raw input symbol sequences. Task-oriented semantic communication is a variant that tries to retain only task-specific information, thus achieving greater bandwidth savings. However, these neural-based communication systems are vulnerable to model inversion attacks, where adversaries try to infer sensitive input information from eavesdropped transmitted data. The key challenge, therefore, lies in preserving privacy while ensuring transmission correctness and robustness. While prior studies typically assume that adversaries aim to fully reconstruct the raw input in task-oriented settings, there exist scenarios where pixel-level metrics such as PSNR or SSIM are low, yet the adversary’s outputs still suffice to accomplish the downstream task, indicating leakage of sensitive information. We therefore adopt the attacker’s task accuracy as a more appropriate metric for evaluating attack effectiveness. To optimize the gap between the legitimate receiver’s accuracy and the adversary’s accuracy, we propose *DiffSem*, a diffusion-aided framework for task-oriented semantic communication. *DiffSem* integrates a transmitter-side self-noising mechanism that adaptively regulates semantic content while compensating for channel noise, and a receiver-side diffusion U-Net that enhances task performance and can be optionally strengthened by self-referential label embeddings. Our experiments demonstrate that *DiffSem* enables the legitimate receiver to achieve higher accuracy, thereby validating the superior performance of the proposed framework.

Index Terms—Semantic communications, diffusion model, privacy preserving, model inversion attack.

I. INTRODUCTION

Deep learning based semantic communication systems have emerged as a promising solution to enhance information transmission efficiency in sixth-generation (6G) wireless networks. Unlike traditional paradigms that prioritize the accurate symbol-level transmission, semantic communication shifts the focus to conveying the intended meaning through symbols [1]. In such systems, the transmitter and receiver collaboratively design mappings between meanings and channel symbols, naturally aligning with the principles of joint source-channel coding (JSCC) [2], [3]. This approach accommodates more complex data sources (e.g., images) and diverse distortion measures, such as classification loss [4] or task-oriented metrics [5]. As a result, semantic communication has been studied for various types of sources such as text [6], [7], visual data [8]–[10], and video [11], [12], and has also been applied in edge computing [13], [14] and autonomous driving [15], [16]. By adopting a “comprehend-first, transmit-later” approach,

The authors are with the School of Science and Engineering, The Chinese University of Hong Kong, Shenzhen, Guangdong 518172, China (e-mail: shyang@cuhk.edu.cn).

semantic communication significantly reduces transmitted data volume, minimizes bandwidth consumption, and improves communication efficiency.

As a variant of semantic communication, task-oriented semantic communication shifts the target from reconstructing the transmitter’s raw input to directly enabling the receiver to accomplish a given task, thereby allowing the transmitter to further compress the transmitted content [17], [18]. For example, in a typical task-oriented semantic communication scenario targeting the image classification task, the sender sends the semantic representation of the picture, and the receiver uses the semantic information to perform the classification task directly, skipping the process of recovering the picture. Studies have demonstrated the efficiency and robustness of task-oriented semantic communication in various scenarios, including image retrieval [19] and federated learning [20], as well as scenarios involving resource-constrained devices [21] and MIMO channels [22].

Despite its advantages, task-oriented semantic communication, like all neural-based systems, is vulnerable to model inversion attacks, in which an adversary eavesdrops on the transmitter’s output and attempts to reconstruct sensitive information of the input [23]. Conventional privacy-preserving techniques, however, are difficult to apply in this context. For example, differential privacy perturbs model inputs or outputs [24], but such perturbations can significantly degrade semantic communication performance [25]. Similarly, federated learning avoids direct data sharing by transmitting parameters, yet remains vulnerable to gradient leakage attacks [26].

Some existing works use adversarial training methods, inspired by the information bottleneck theory, that aim to reduce the pixel-level quality of reconstructions [27]–[29], using image-quality metrics such as peak signal-to-noise ratio (PSNR) or structural similarity index measure (SSIM). From an information-theoretic perspective, requiring an adversary to fully reconstruct the original data is not well-founded, as the transmitter never conveys sufficient information to enable exact recovery. In fact, preventing input reconstruction merely requires constraining the transmitted information to contain only task-relevant features, without the need for additional countermeasures.

Motivated by this observation, we consider a generalized notion of model inversion attacks: an attack is deemed successful if the adversary can reconstruct sensitive information that is sufficient to accomplish the task. For classification tasks, this definition corresponds to evaluating the accuracy of the adversary’s reconstruction under a strong classifier [17], similar to the concept of “semantic fidelity” in [17], [30].

We revisit part of the aforementioned work and argue that their proposed defenses [29], [31] are in fact weak. Even when pixel-level reconstructions appear poor, an adversary may still succeed if the recovered semantics are sufficient for the task. Conversely, restricting task-agnostic recoverability while preserving task-specific semantics provides a principled means of protecting privacy, which is aligned with the analysis in [32]. Building on this perspective, we revisit the notion of privacy: in task-oriented systems, we argue that privacy should be measured by the performance gap between the legitimate receiver and the adversary. In other words, the source of privacy lies in the information asymmetry between them.

This paper proposes *DiffSem*, a diffusion-aided task-oriented semantic communication system which enhances task performance while limiting adversarial recovery. A diffusion model is a generative architecture that learns to recover the original data distribution from noise through forward noising and reverse denoising [33], [34]. Such models have been applied to tasks such as audio restoration and image denoising within semantic communication, where conditional diffusion and receiver-side guidance are typically employed to help the receiver refine its reconstructions [35]–[38]. However, in privacy-preserving semantic communication systems, the receiver’s task can be confidential, that is, neither the transmitter nor potential adversaries are allowed to access task information [39]. To make sure that *DiffSem* works in the confidential scenario, it couples a transmitter-side self-noising module that adaptively regulates how much task-specific feature is observable while compensating for channel noise, with a guidance-free receiver diffusion U-Net that enhances task performance under dynamic channels; the receiver can be further strengthened by self-referential label embeddings while remaining guidance-free. Conceptually, the self-noising module exploits the semantic-information mismatch: it reduces task-agnostic recoverability from the transmitted features without depriving a task-aware receiver of the semantics needed for the downstream task.

In general, our contributions can be summarized as follows.

- We generalize the notion of model inversion attack by defining its success in terms of the attacker’s task accuracy rather than pixel-level similarity. Experiments show that even when reconstructions have low PSNR or SSIM, attackers can still achieve high task accuracy, indicating that conventional defenses focused on image pixel-level quality are largely weak.
- We develop a non-adversarial privacy mechanism that exploits the intrinsic mismatch between the semantics needed by the legitimate task and the broader content an attacker must reconstruct. By limiting task-agnostic recoverability while preserving task-specific semantics, our approach mitigates model inversion without the utility loss associated with adversarial training.
- We propose *DiffSem*, a diffusion-aided semantic communication framework for scenarios where the receiver’s task is confidential. *DiffSem* introduces a transmitter-side self-noising mechanism that adaptively regulates the radiated semantic information to compensate for channel noise, and a guidance-free receiver-side diffusion U-

Net that enhances task performance. An optional self-referential label embeddings further improves performance without violating the guidance-free constraint. Our experiments on MNIST and CIFAR-10 datasets show that *DiffSem* significantly increases the legitimate receiver’s accuracy.

This paper is organized as follows. Section II describes the task-oriented semantic architecture as well as the model inversion attack, and general evaluations of the system. Section III introduces the modules and the training algorithms in our system in detail. Section IV includes the experiment results and discussion. Section V concludes the paper.

II. SYSTEM ARCHITECTURE

In this section, we first describe the overall system architecture and then analyze model inversion attacks as a representative privacy threat. Finally, we introduce the evaluation framework used to quantify the privacy guarantees of our design.

A. Diffusion based Task-oriented Semantic System

As shown in Fig. 1(a), assume there is a task-oriented transmitter-receiver pair that performs a specific task using the input raw data x to get target output y . First, $x \in X$ is sent into a feature extractor module and a channel coding module to get neural-coded features $f \in F$. In our system, these two modules are both implemented by neural networks, and they can be regarded as a whole module named encoder Φ_ϕ with parameter set ϕ , like any other neural-network based joint-source-channel-coding (JSCC) system in related literature. Next, a self-noising module Ψ is utilized to add a certain level of noise, based on system requirements, to get z that is ready to transmit. These steps can be expressed as

$$z = \mathcal{T}_\phi(x) = \Psi(\Phi_\phi(x)) = \Psi(f) \quad (1)$$

where \mathcal{T} means the transmitter. Note that the self-noising module Ψ does not have any learnable parameters; details are introduced later.

Assuming additive white Gaussian noise (AWGN) channel is used¹. After transmitting over the air, the receiver first observes the complex-baseband signal

$$\hat{z} = z + \epsilon, \quad (2)$$

where $\epsilon \sim \mathcal{N}(0, \sigma^2 \mathbf{I})$ is additive white Gaussian noise (AWGN) in the wireless channel \mathcal{C} . Then, \mathcal{R} performs its task in two steps. First, it uses a diffusion module Δ_δ to get the estimated feature \hat{f} through denoising; second, \hat{f} is channel decoded and is used to perform a specific task. Decoding and task execution are also combined into a single module, referred to as the classifier Θ_θ , analogous to the encoder module introduced above. Hence the receiver is defined as

$$\hat{y} = \mathcal{R}_{(\delta, \theta)}(\hat{z}) = \Theta_\theta(\Delta_\delta(\hat{z})) = \Theta_\theta(\hat{f}), \quad (3)$$

¹Our model also covers block fading channel [40] with receiver’s channel state information (CSI). Consider x being transmitted within a block, a one-tap coherent equalizer maps $\hat{z} = hz + \epsilon$ to $z + \tilde{\epsilon}$ where the noise variance of $\tilde{\epsilon}$ is rescaled by $1/|h|^2$ compared to ϵ [8], [41], [42]. We leave a detailed treatment of fading channels to our future work.

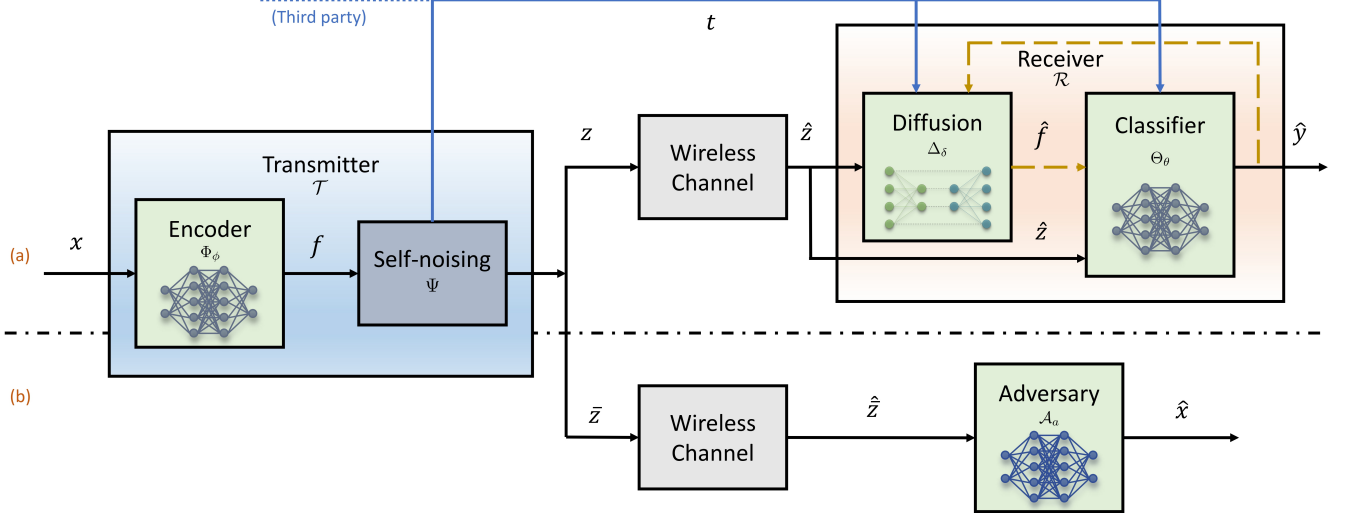


Fig. 1: System models. (a) Task-oriented transmission system. (b) Model inversion attack by adversary.

where δ and θ are the parameter sets in denoising module Δ_δ and classifier module Θ_θ , respectively, and \hat{y} is the task output. Note that in wireless transmissions, $z, \hat{z} \in \mathbb{C}^\kappa$, where κ means complex channel use. Since neural networks only process real numbers, without further notice, let $k = 2\kappa$, and the length of z (f as well) is k in our system's implementation.

Remarks. We assume that there is a trustworthy third party that can define the specific task and arrange models in each node of the system. Thus, we define that Θ_θ is reachable only in \mathcal{R} when models are trained and deployed by the third-party, which is a common prerequisite in task-oriented communications [43].

B. Model Inversion Attack

Model inversion attack, proposed by Fredrikson et al. [44], is a representative *threat model* in which an adversary attempts to reconstruct sensitive input information from the outputs of a machine learning model. In semantic communication systems, the concern about model inversion attack has been explicitly raised in [29]. In their setting, an adversary continuously queries the semantic transmitter to obtain noisy features, and then trains an inversion model to recover private inputs. They adopt a black-box adversarial assumption and employ mean squared error (MSE) as the reconstruction metric. Motivated by these findings, we now formalize the threat model for JSCC-based semantic communications under the following assumptions [45]:

- **Black-box access.** The adversary \mathcal{A}_a has no access to the model parameters or the training dataset of the transmitter \mathcal{T} .
- **Distribution mismatch.** Unlike the legitimate transmitter, \mathcal{A}_a does not possess data drawn from the same distribution as X , and must construct a surrogate dataset \hat{X} from a related but mismatched distribution.
- **Chosen-plaintext attack.** \mathcal{A}_a may freely construct input samples $\hat{x} \in \hat{X}$, obtain the corresponding post-channel

outputs \hat{z} delivered by \mathcal{T} , and collect sufficient pairs $\{\hat{x}, \hat{z}\}$ to train itself, as shown in Fig. 2.

We also employ the wireless settings similar to [12], such that \mathcal{A}_a can only eavesdrop on the communication link rather than directly observe the output of the model. As shown in Fig. 1(b), \mathcal{A}_a observes \hat{z} on a separate channel and attempts to reconstruct the transmitted symbol x . This is modeled as

$$\hat{x} = \mathcal{A}_a(\hat{z}) = \mathcal{A}_a(\bar{z} + \epsilon), \quad (4)$$

where $\epsilon \sim \mathcal{N}(0, \sigma^2 \mathbf{I})$ denotes the noise in the adversary channel, and a is the parameter set of \mathcal{A}_a . To train its inversion model, \mathcal{A}_a minimizes the reconstruction distortion using the MSE loss:

$$\mathcal{L}_{\text{MSE}}(x_i, \hat{x}_i) = \frac{1}{M} \sum_{i=1}^M \|x_i - \hat{x}_i\|^2. \quad (5)$$

C. System Performance Evaluation

In this paper, we assume that the receiver performs an image classification task, so that \mathcal{R} is trained using the cross-entropy (CE) loss

$$\mathcal{L}_{\text{CE}}(\phi, \theta) = - \sum_i p(y_i) \log q(\hat{y}_i), \quad (6)$$

where $p(y)$ and $q(\hat{y})$ denote the true and predicted label distributions, respectively. The classification accuracy is the fraction of correctly classified inputs.

Pixel-level evaluations. Since the adversary \mathcal{A}_a aims to estimate source images, pixel metrics such as PSNR and SSIM are often employed:

$$\text{PSNR} = 10 \log_{10} \left(\frac{R^2}{\text{MSE}} \right), \quad (7)$$

$$\text{SSIM}(x, \hat{x}) = \frac{(2\mu_x \mu_{\hat{x}} + c_1)(2\sigma_{x\hat{x}} + c_2)}{(\mu_x^2 + \mu_{\hat{x}}^2 + c_1)(\sigma_x^2 + \sigma_{\hat{x}}^2 + c_2)}, \quad (8)$$

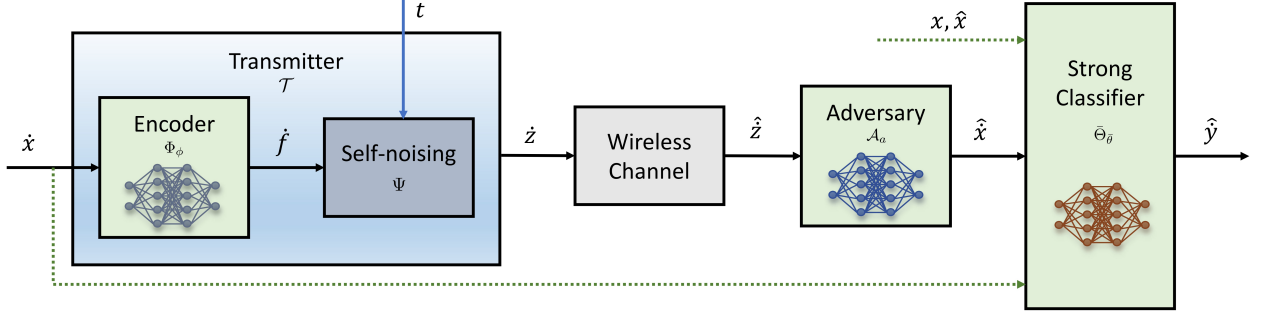


Fig. 2: The adversary prepares its dataset and accesses the transmitter repeatedly, with a well-trained strong classifier evaluating its outputs. Green dashed lines indicate the datasets that are used to train the strong classifier.

where R is the maximum pixel value (e.g., 255 for 8-bit images), MSE is the mean squared error, μ_x and $\mu_{\hat{x}}$ are the average pixel values of x and \hat{x} , σ_x^2 and $\sigma_{\hat{x}}^2$ are the variances of x and \hat{x} , $\sigma_{x\hat{x}}$ is the covariance between x and \hat{x} , and c_1, c_2 are small constants that stabilize the division and avoid zero denominators. Higher PSNR indicates better perceptual quality between the reconstructed and reference images. SSIM takes values in $[-1, 1]$ but typically lies within $[0, 1]$ in practice, with larger values corresponding to higher structural similarity.

Strong classifier aided evaluation. Here we introduce a strong classifier $\bar{\Theta}_{\bar{\theta}}$, whose architecture is deliberately larger and more expressive than the receiver's classifier Θ_{θ} , so that it can serve as a reliable module for evaluation. $\bar{\Theta}_{\bar{\theta}}$ is pretrained using training set including x , \hat{x} , and x and \hat{x} and corresponding labels to categorize into the ground-truth label \hat{y} ². The strong classifier is never involved in training or inference of the system in Fig. 1; instead, it is only applied after transmission to assess the quality of the adversary's reconstructions, as shown in Fig. 2. The role of $\bar{\Theta}_{\bar{\theta}}$ is to provide a reference that, if an attacker's reconstruction still contains sufficient task-relevant semantics, the strong classifier is expected to classify them correctly. In this way, both the ordinary classifier Θ_{θ} at the receiver side and the stronger evaluator $\bar{\Theta}_{\bar{\theta}}$ yield accuracies that can be directly compared, offering a clear measure of semantic fidelity.

III. MODULES AND TRAINING

In this section, we first introduce each module in our system together with data flow, followed by a detailed description of the training procedure based on the system design.

A. Encoder, Classifier and Adversary Modules

In our system, encoder module Φ_ϕ extracts neural-coded feature f whose shape is $\sqrt{k} \times \sqrt{k}$ from source images x^{CHW} with channel C , height H and width W , and the compression rate is $\rho = k/(CHW)$. Feature f is self-distorted to z and is transmitted over the air, then the receiver gets channel-interfered signal \hat{z} . Receiver uses denoising module Δ_δ and classifier module Θ_θ to generate \hat{y} .

²For simplicity, outputs of $\bar{\Theta}_{\bar{\theta}}$ are all denoted as \hat{y} .

In related work [29], an auxiliary decoder \mathcal{D} is commonly introduced to simulate an attacker during training, particularly in the context of adversarial learning frameworks. However, our approach does not adopt such attacker-aware training strategies. Instead, we define \mathcal{A}_a as a model trained via model inversion attacks, solely for the purpose of evaluating the privacy risks after the transmission model is established. Importantly, \mathcal{A}_a is not allowed to participate in the training or inference of the transmitter \mathcal{T} and receiver \mathcal{R} . Likewise, if \mathcal{D} is used in other methods, it should be restricted to the training phase and excluded from the evaluation phase. In our framework, since no adversarial training is involved, the auxiliary decoder \mathcal{D} is entirely omitted. The strong classifier $\bar{\Theta}_{\bar{\theta}}$, as mentioned above, is employed solely for evaluation of \mathcal{A}_a .

B. Diffusion Module

We use denoising diffusion implicit models (DDIM) [46] to train the diffusion module in our system. Unlike conventional generative usage, we adopt a paired design in which the transmitter deliberately applies a partial forward diffusion (self-noising) to f_0 up to a controllable step T' , while the receiver runs a matching DDIM reverse schedule to deterministically denoise back toward f_0 . This coupling makes T' an information knob that jointly governs utility and privacy. In the forward process, diffusion module gradually adds Gaussian noise to the extracted feature f with a series of schedules $\alpha_1, \dots, \alpha_T \in [0, 1]$. To avoid ambiguity and facilitate discussion, in this section, let f_0 represent $f \in \mathcal{F}$ mentioned earlier; that is, $f_0 \sim p(f_0)$ denotes the original feature, which is the output of encoder Φ_ϕ and is not distorted yet. Then, noisy versions f_1, \dots, f_T are obtained by the following process in T steps [33]:

$$p(f_t | f_{t-1}) = \mathcal{N}(f_t; \sqrt{1 - \alpha_t} f_{t-1}, \alpha_t \mathbf{I}), \forall t \in \{1, \dots, T\}, \quad (9)$$

where \mathbf{I} is the identity matrix that has the same dimensions as f_0 , and $\mathcal{N}(f_t; \mu, \sigma)$ is the normal distribution of mean μ and covariance σ that generates f_t .

This recursive formulation allows f_t to be sampled directly

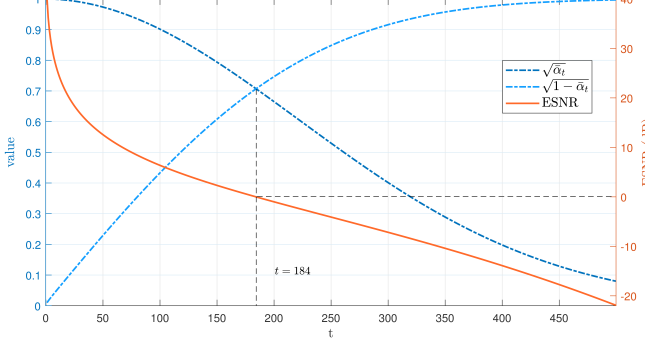


Fig. 3: Changes of $\sqrt{\bar{\alpha}_t}$, $\sqrt{1 - \bar{\alpha}_t}$ and p with t .

from

$$p(f_t|f_0) = \mathcal{N}(f_t; \sqrt{\bar{\alpha}_t} f_0, (1 - \bar{\alpha}_t) \mathbf{I}), \quad t \sim \mathcal{U}\{1, \dots, T\}, \quad (10)$$

where \mathcal{U} draws a normal distribution, $\bar{\alpha}_t = \prod_{i=1}^t \beta_i$ and $\beta_t = 1 - \alpha_t$. Then we have

$$f_t = \sqrt{\bar{\alpha}_t} f_0 + \sqrt{1 - \bar{\alpha}_t} \epsilon_t, \quad (11)$$

where $\epsilon_t \sim \mathcal{N}(0, \mathbf{I})$, to sample f_t from $p(f_t|f_0)$ in the diffusion module's training step.

To ease the training and using of diffusion module, we choose $(\alpha_t)_{t=1}^T$ to be linear increasing constants, that is

$$\alpha_t = \alpha_1 + \left(\frac{\alpha_T - \alpha_1}{T - 1} \right) (t - 1), \quad (12)$$

where $\alpha_1 = 10^{-4}$, $\alpha_T = 2 \times 10^{-2}$. We train the diffusion module using $T = 500$, but $T' < T$ is used in the experiment to test the system's robustness. The values of $\sqrt{\bar{\alpha}_t}$ and $\sqrt{1 - \bar{\alpha}_t}$ varying by t are shown in Fig. 3. We plot the “ESNR” line that is defined by

$$\mathcal{P} = \frac{\mathbb{E}(\|\sqrt{\bar{\alpha}_t} f_0\|^2)}{\mathbb{E}(\|\sqrt{1 - \bar{\alpha}_t} \epsilon_t\|^2)}, \quad (13)$$

where \mathcal{P} represents the power ratio between the signal component $\sqrt{\bar{\alpha}_t} f_0$ and noise component $\sqrt{1 - \bar{\alpha}_t} \epsilon_t$ obtained after partially adding noise, and varies with the values of α_1 , α_T and T . In our system, f_0 is power-normalized after generated by encoder Φ_ϕ . Hence, according to Eq. (13), it is equivalent to the signal f_0 passing through an AWGN channel with signal-to-noise ratio \mathcal{P} , which we refer to as “equivalent SNR” (ESNR). As an example, we marked the point $t = 184$ in Fig. 3, where the energy of the signal component is approximately equal to that of the noise component, and the ESNR $p = 0.01$ dB $\simeq 0$ dB.

Design rationale. The transmitter stops the forward diffusion at T' and the receiver runs the reverse schedule anchored at the same grid, so the receiver sees a corruption level consistent with its reverse schedule, which makes T' a trade-off parameter between system utility and attacker difficulty. In practice, T' is chosen once and reused across samples; DDIM's snapped timestep grid further makes this setting robust to small SNR variations.

The signal \hat{z} needs to be denoised first on the receiver side. Usually, a deep learning network called U-Net can be used to

predict ϵ_t during the sample process. U-Net is a convolutional neural network that can effectively handle multi-scale features and reconstruct high-fidelity output during the reverse process. U-Net learns to estimate f_0 from f_t and t by minimizing the difference between the predicted noise

$$\epsilon_{f_t} = \Delta_\delta(f_t, t) \quad (14)$$

and the actual noise ϵ_t , and is trained using the MSE loss of these two noises, denoted by [33]

$$\mathcal{L}_{\text{U-Net}} = \mathbb{E}_{t \sim [1, T]} \mathbb{E}_{f_0 \sim p(f_0)} \mathbb{E}_{\epsilon_t \sim \mathcal{N}(0, \mathbf{I})} \|\epsilon_{f_t} - \epsilon_t\|^2. \quad (15)$$

With a well-trained U-Net, the goal is to progressively denoise f_t and to recover f_0 starting from a latent variable $f_T \sim \mathcal{N}(0, \mathbf{I})$. Specifically, on step $t - 1$, given f_t and ϵ_t , we have

$$f_{t-1} = \sqrt{\bar{\alpha}_{t-1}} \left(\frac{f_t - \sqrt{1 - \bar{\alpha}_t} \epsilon_{f_t}}{\sqrt{\bar{\alpha}_t}} \right) + \sqrt{1 - \bar{\alpha}_{t-1}} \epsilon_{f_t}. \quad (16)$$

To generate samples efficiently, DDIM uses a deterministic, stride-based reverse schedule over a subset $\{t_1 > \dots > t_N\} \subseteq \{1, \dots, T\}$ with $N \ll T$. In our paired design, the receiver's schedule *snaps* the target step T' to the nearest element in this grid.

A diffusion model learns the distribution $p(f_0)$ rather than an exact per-sample inverse. When initialized from pure noise, it only ensures sampling from the learned distribution and thus cannot guarantee recovery of the specific input instance. However, communication demands recoverability of the transmitted semantics. Our paired design resolves this tension: the transmitter halts the forward diffusion early (self-noising at T') so that sufficient task-relevant structure remains in $f_{T'}$, and the receiver runs the matching reverse schedule to deterministically peel off the injected noise. Optional guidance then further biases the reverse trajectory toward the intended task.

Transmitter-side self-noising. Let $0 \leq T' \leq T$, and perform

$$f_{T'} = \sqrt{\bar{\alpha}_{T'}} f_0 + \sqrt{1 - \bar{\alpha}_{T'}} \epsilon_{T'}, \quad (17)$$

in the self-noising module Ψ before transmitting. In the receiver, Δ_δ tries to recover f_0 using T' steps' iteration that is the same as Eq. (16). This gives a way to control the weight of “task-relevant information” $\sqrt{\bar{\alpha}_{T'}} f_0$ in the distorted output. The larger T' is, the less “task-relevant information” in $f_{T'}$, and nearly no guidance involved when $T' = T$ (in which diffusion module generates f_0 without specific order). Since Eq. (17) is valid for any $0 \leq T' \leq T$, we can train the diffusion module to denoise from T and deploy the well-trained module that is set by T' when transmitting the signal, while receiver recovers the estimation of f_0 without other explicit guidance required. In this way, the choice of T' controls the distortion of the transmitter, hence affects the difficulty for adversaries to estimate the original images with task information in them.

To further enhance system performance, the receiver can utilize self-generated label guidance. Specifically, the classifier module Θ_θ generates the output \hat{y} bypassing the diffusion module Δ_δ at first. The accuracy of \hat{y} is higher when distortion on f is lower or channel condition is favorable, which means

that \hat{y} could be more helpful in such cases. Then \hat{y} can be used to guide the diffusion module Δ_δ in the denoising process (Fig. 1). Different from calculating the accuracy of \hat{y} , here we use the soft version of \hat{y} that all the category info in the vector will be utilized as guidance. Next, \hat{z} and \hat{y} are fed into Δ_δ to produce \hat{y}' , which is further reintroduced into Δ_δ for refined denoising. By iterating this feedback loop multiple times, the accuracy of \mathcal{R} is significantly improved. Consistent with guidance-based DDIM implementation, we provide explicit external control to Δ_δ by modifying the noise estimation in Eq. (14) to

$$\epsilon_{(f_t, \hat{y})} = \Delta_\delta(f_t, \hat{y}, t), \quad (18)$$

where \hat{y} serves as self-referential guidance. During the training, a classifier-free DDIM is trained with ground-truth labels y by replacing the term ϵ_{f_t} with $\epsilon_{(f_t, y)}$ in Eq. (15). During sampling, \hat{y} replaces y to adaptively guide denoising. This soft label-embedding method ensures that:

- If \hat{y} is more accurate, the denoising effect is enhanced;
- If \hat{y} is unreliable (e.g., due to excessive self-noising in Ψ or poor channel conditions), the system performance remains stable without degradation.

Although the external guidance from \hat{y} may be suboptimal in extreme cases, it improves robustness in most scenarios. Detailed experimental validation of this iterative denoising framework is provided in Sec. IV.

C. Diffusion Module Under Wireless Channel

Here we discuss the impact of wireless channel on the diffusion module in our system. To facilitate discussion, let $f_{T'} = z'$, then the receiver gets

$$z' = z' + \epsilon_{\text{ch}} = (\sqrt{\bar{\alpha}_{T'}} f_0 + \sqrt{1 - \bar{\alpha}_{T'}} \epsilon_{T'}) + \epsilon_{\text{ch}}, \quad (19)$$

where $\epsilon_{\text{ch}} \sim \mathcal{N}(0, \sigma_{\text{ch}}^2 \mathbf{I})$ represents channel noise. Obviously, the channel noise term adds extra distortion to $f_{T'}$ and changes its distribution, thus affects the sampling process at the receiver. To tackle this issue, we introduce a noise margin for possible channel interference during the forward process.

Suppose we need to distort f_0 to $f_{T'}$ which will be transmitted at \mathcal{T} , given specific timestep T' . Let $0 \leq T'' < T'$ and

$$f_{T''} = \sqrt{\bar{\alpha}_{T'}} f_0 + \sqrt{1 - \bar{\alpha}_{T''}} \epsilon_{T''}, \quad (20)$$

where $\epsilon_{T''} \sim \mathcal{N}(0, \mathbf{I})$. Note that the first term of $f_{T''}$ remains the same as that of $f_{T'}$. For simplicity, let $\epsilon_{T'} = \epsilon_{T''} = \epsilon$. Then, \mathcal{T} transmits $f_{T''}$ to the wireless channel, and receiver obtains

$$\hat{z}'' = z'' + \epsilon_{\text{ch}} = \sqrt{\bar{\alpha}_{T'}} f_0 + \sqrt{1 - \bar{\alpha}_{T''}} \epsilon + \epsilon_{\text{ch}}. \quad (21)$$

If

$$\mathbb{E}(\|\sqrt{1 - \bar{\alpha}_{T'}} \epsilon\|^2) = \mathbb{E}(\|\sqrt{1 - \bar{\alpha}_{T''}} \epsilon + \epsilon_{\text{ch}}\|^2), \quad (22)$$

then $\mathbb{E}(\|\hat{z}''\|^2) = \mathbb{E}(\|z'\|^2)$, which is equivalent to that \mathcal{R} receives $f_{T'}$. So we can transmit z'' while maintaining the distribution after the wireless transmission, and then the

diffusion module can recover the estimation of f_0 without further ambiguity.

Now we need to find T'' . Let γ denote channel's signal-to-noise power ratio (SNR), then we have

$$\sigma_{\text{ch}}^2 = \frac{\mathbb{E}(\|z''\|^2)}{\gamma} = \frac{\bar{\alpha}_{T'} \mathbb{E}(\|f_0\|^2) + (1 - \bar{\alpha}_{T''}) D}{\gamma}, \quad (23)$$

where D is the length of ϵ and $\mathbb{E}(\|\epsilon\|^2) = D$.

By considering Eq. (21) to (23), we can derive that

$$\bar{\alpha}_{T''} = \frac{\bar{\alpha}_{T'} (\gamma + \mathbb{E}(\|f_0\|^2)) + D}{\gamma + D}. \quad (24)$$

Details can be found in Appendix A. In Eq. (24), $\bar{\alpha}_t$ can be regarded as a discrete function of t according to Eq. (12), so T'' can be approximated given T' , γ and f_0 ³. In this way, our diffusion module can effectively handle the effects of the wireless channel⁴.

Remark on SNR estimation (and sampler insensitivity). In the implementation, we simply substitute an estimate \hat{y} for γ in Eq. (23)–(24). With a deterministic, stride-based DDIM sampler, the reverse process runs on a fixed discrete timestep sequence $\{t_1 < \dots < t_N\} \subseteq \{1, \dots, T\}$ (e.g., $t_i = 10(i - 1)$ for a 500-step DDPM schedule gives $[0, 10, 20, \dots, 500]$ under zero-based indexing). Consequently, the continuous target implied by Eq. (24) is effectively quantized to the nearest grid point when selecting T'' . Small SNR mismatches typically unlikely to change the snapped index. In contrast, finely stepped stochastic DDPM schedules can be more sensitive to such perturbations. Hence, precise SNR estimation is *not* necessary for our method, as imprecise estimation only shifts the operating point marginally without affecting our conclusions.

D. System Training Procedure

Here we introduce the training procedure in our experiment. As shown in Fig. 1, t is used as a global parameter that controls the distortion at the transmitter and helps the denoising at the receiver. All modules are neural-based except for self-noising module and wireless channel modules. The self-noising module can be regarded as a channel compensator, ensuring that the signals received by the diffusion module appear as if they have passed through a Gaussian channel, thereby conforming to the input requirements for denoising. MNIST and CIFAR-10 are used as datasets to train the system model. Given the small size of images and features in these datasets, we only employ a simple diffusion module that is easy to train and implement, as well as convenient for deployment considering the low-latency requirements of practical communication systems.

For ease of tracking, we divide the training procedure into two parts. The first part consists of three stages, each designed to prepare a specific module, as outlined in Algorithm 1. We assume that when an adversary \mathcal{A}_a attempts to “join” a transmitter-receiver pair, the transmitter \mathcal{T} and receiver \mathcal{R} have

³ f_0 and ϵ_{ch} are of the same length.

⁴In the implementation, we find the maximum T'' that $\alpha_{T''}$ is no larger than the right side of Eq. (24). If not, set $T'' = 0$; generally, it means that T' is small enough, or γ is larger enough. Both situations mean that there will not be significant distortion on f_0 .

Algorithm 1 System Training Preparation

- 1: **Initialization:** Initialize weights W and biases b in \mathcal{T} , \mathcal{R} , \mathcal{A}_a and $\bar{\Theta}_{\bar{\theta}}$.
- 2: **Input:** $x \in X$ and $\dot{x} \in \dot{X}$.
- 3: **Stage 1: Training Φ_{ϕ} and Θ_{θ} .**
- 4: $\Phi_{\phi}(x) = z$.
- 5: Transmit z over wireless channel and get \hat{z} .
- 6: $\Theta_{\theta}(z) = \hat{y}$.
- 7: Calculate \mathcal{L}_{CE} by Eq. (6) and update ϕ , θ .
- 8: **Stage 2: Training Δ_{δ}**
- 9: $\Phi_{\phi}(x) = f$.
- 10: Train U-Net by minimizing $\mathcal{L}_{U\text{-Net}}$ using Eq. (15), and update δ .
- 11: **Stage 3: Training \mathcal{A}_a and $\bar{\Theta}_{\bar{\theta}}$**
- 12: $\Phi_{\phi}(\dot{x}) = \dot{z}$.
- 13: Transmit \dot{z} over wireless channel and get $\hat{\dot{z}}$.
- 14: $\mathcal{A}_a(\hat{\dot{z}}) = \hat{x}$.
- 15: Directly distort x to get \ddot{x} .
- 16: $\bar{\Theta}_{\bar{\theta}}([x; \dot{x}; \hat{x}; \ddot{x}]) = \hat{y}$.
- 17: Use \hat{x} to calculate MSE loss by Eq. (5); use \hat{y} to calculate CE loss by Eq. (6).
- 18: Update a and $\bar{\theta}$.
- 19: **Output:** Pre-trained network \mathcal{T} , \mathcal{R} , \mathcal{A}_a and $\bar{\Theta}_{\bar{\theta}}$.

Algorithm 2 Receiver Fine-tuning

- 1: **Initialization:** Load pre-trained networks \mathcal{T} , \mathcal{R} and \mathcal{A}_a .
- 2: **Input:** $x \in X$.
- 3: **Given** $0 \leq T' \leq T$,
- 4: Find T'' by Eq. (24).
- 5: $\mathcal{T}_{\phi}(x, T', T'') = z$.
- 6: Transmit z over wireless channel and get \hat{z} .
- 7: $\Theta_{\theta}(\hat{z}, T') = \hat{y}$.
- 8: **if** using E-DiffSem:
- 9: **while** accuracy of \hat{y} increases:
- 10: **for** $t \in \{t_1 = 0 < t_2 < \dots < t_N = T'\}$:
- 11: Denoise \hat{z} by Eq. (16) and Eq. (18) from f_t to f_{t-1} , with \hat{y} involved.
- 12: **end for** and get \hat{f} .
- 13: $\Theta_{\theta}(\hat{f}, \hat{z}, T') = \hat{y}$.
- 14: **end while**
- 15: **elif** using DiffSem:
- 16: **for** $t \in \{t_1 = 0 < t_2 < \dots < t_N = T'\}$:
- 17: Denoise \hat{z} by Eq. (16) and Eq. (14) from f_t to f_{t-1} .
- 18: **end for** and get \hat{f} .
- 19: $\Theta_{\theta}(\hat{f}, \hat{z}, T') = \hat{y}$.
- 20: **end if**
- 21: Calculate $\mathcal{L}_{CE}(y, \hat{y})$ by Eq. 6 and update θ .
- 22: Change T' and return to Line 3 to repeat.
- 23: **Output:** Finetuned network Θ_{θ} .

already been fully trained and are successfully deployed on the transmission nodes. Consequently, the training of \mathcal{A}_a must occur after the completion of the \mathcal{T} - \mathcal{R} pair. As shown in Fig. 2, we use the well-trained transmitter to train the adversary, where receiver is not involved here. Hence, the performance of \mathcal{A}_a will inherently depend on the training outcomes of \mathcal{T} .

TABLE I
SUMMARY OF MODULES FOR MNIST DATASET

Modules	Layers	Output Dimensions
Encoder	Conv2d+LeakyReLU	$16 \times 14 \times 14$
	Conv2d+LeakyReLU	$32 \times 8 \times 8$
	Conv2d+LayerNorm	$1 \times 8 \times 8$
Classifier (in Receiver)	Linear+ReLU	$64 \times 2+1$
	Linear	10
Strong Classifier (in Third-party)	Linear+Tanh	784
	Linear+Tanh	128
	Linear+Sigmoid	10
Adversary	Linear+Tanh	784
	Linear	$1 \times 28 \times 28$

By optimizing the training of the \mathcal{T} - \mathcal{R} pair and subsequently training \mathcal{A}_a to its fullest potential, we aim to limit the amount of valid information that the adversary can extract under the given dataset and system. The training of strong classifier $\bar{\Theta}_{\bar{\theta}}$ can be carried out simultaneously with \mathcal{A}_a , or after the training of \mathcal{A}_a is finished.

The second part is fine-tuning the receiver given fixed Φ_{ϕ} and Ψ , as described in Algorithm 2. We implemented DiffSem, which performs a single-pass pipeline processing on the receiver's input, and an enhanced version named E-DiffSem, where "E" stands for "enhance". E-DiffSem utilizes soft \hat{y} as self-referential guidance to improve the performance of denoising. Specifically, self-referential \hat{y} is iteratively utilized until the accuracy of \hat{y} reaches stability. For both methods, the diffusion steps N are set to $\min(T', 50)$. Experimental results and discussions will be elaborated in the next section.

IV. EXPERIMENTS AND RESULTS

In this section, we will first explain the module design in our system and introduce the details of experiment initialization. Next, we present the results and discussions based on our experimental findings.

A. Module Implementation

The structures of modules involved in our system are as shown in Table I and Table II. Functions of each module are as mentioned above. The compression rates (ρ) are set to 8.16% and 6.25% for the MNIST and CIFAR-10 datasets, respectively. These values are chosen merely for the convenience of model training, without any specific or intentional numerical design. Note that before the encoder's output is sent to the self-noising module, it undergoes power normalization to make sure that $\sum_i(f_i^2/k) \leq 1$, where i is the pixel index. This operation is performed during the training of the \mathcal{T} - \mathcal{R} pair and the training of Δ_{δ} , to facilitate the denoising process at the receiver. Therefore, the output of the \mathcal{T} does not require further normalization.

There are two classifiers in the system, Θ_{θ} and stronger $\bar{\Theta}_{\bar{\theta}}$. When using the MNIST dataset, the input of Θ_{θ} is a combination of \hat{z} , \hat{f} and t , resulting in a dimension of $64 \times$

TABLE II
SUMMARY OF MODULES FOR CIFAR-10 DATASET

Modules	Layers	Output Dimensions
Encoder	Conv2d+LeakyReLU	$16 \times 32 \times 32$
	Conv2d+LeakyReLU	$32 \times 16 \times 16$
	Residual	$32 \times 16 \times 16$
	Conv2d+LeakyReLU +LayerNorm	$3 \times 8 \times 8$
Classifier (in Receiver)	Conv2d+Tanh	$64 \times 8 \times 8$
	Conv2d+Tanh	$512 \times 4 \times 4$
	Residual Block	$512 \times 4 \times 4$
	AdaptiveAvgPool2d	512
	Linear+Tanh	10
Strong Classifier (in Third-party)	Conv2d+ReLU	$64 \times 32 \times 32$
	Conv2d+ReLU	$256 \times 16 \times 16$
	Residual Block	$512 \times 8 \times 8$
	AdaptiveAvgPool2d	$512 \times 2 \times 2$
	Linear+ReLU	256
	Linear	10
Adversary	Conv2d+Tanh	$512 \times 8 \times 8$
	(ConvTrans2d+Tanh +Residual Block) $\times 2$	$128 \times 32 \times 32$
	Conv2d+Tanh	$3 \times 32 \times 32$

TABLE III
SUMMARY OF STRUCTURE FOR U-NET

Steps	Layers	Output Dimensions
Encoding	ResidualConv Block	$128 \times 8 \times 8$
	Unet Down	$128 \times 4 \times 4$
	Unet Down	$256 \times 2 \times 2$
Vectorization	AvgPool2d+GELU	$768 \times 1 \times 1$
Embedding	2 \times EmbedFC (Time)	$(256/128) \times 1 \times 1$
	2 \times EmbedFC (Context)	$(256/128) \times 1 \times 1$
Decoding	ConvTrans2d +GroupNorm+ReLU	$256 \times 2 \times 2$
	UnetUp	$128 \times 4 \times 4$
	UnetUp	$128 \times 8 \times 8$
Output	Conv2d+GroupNorm +ReLU+Conv2d	$1 \times 8 \times 8$

$2+1$, while the input size of $\bar{\Theta}_{\bar{\theta}}$ is $1 \times 28 \times 28$. For the CIFAR-10 dataset, the input of Θ_{θ} is a concatenation of \hat{z} and \hat{f} , with t padded alongside them. Hence, the dimension of the input becomes $(3 \times 2) \times 8 \times (8+1) = 6 \times 8 \times 9$. The strong classifier $\bar{\Theta}_{\bar{\theta}}$ needs to learn from the combined dataset that includes x , \hat{x} and \hat{z} , and aims to achieve as accurate classification as possible. $\bar{\Theta}_{\bar{\theta}}$ also learns to categorize images that are directly distorted according to channel conditions, denoted as \ddot{x} .

The structure of U-Net in the diffusion module is shown in Table III⁵. We employ U-Net to denoise the input effectively

⁵Due to limited space and to avoid excessive repetition, here we present the structure of U-Net used in E-DiffSem. For DiffSem, context embedding is not involved, the vectorization step generates $128 \times 2 \times 2$, and the output dimensions with 256 should be 128.

while incorporating the guide information. Specifically, it first processes noisy features by down-sampling them through an encoding step. The down-sampled features are then vectorized and combined with time embeddings and context embeddings (if any) that guide the decoding step. Decoding step up-samples the features and integrates skip connections from the encoding. Finally, convolutional layers reconstruct the denoised features that match the input dimensions. This structure allows the model to effectively denoise images while incorporating time and context information. In our implementation, the diffusion module remains static after training, allowing pre-trained diffusion models to handle and generate transmission information efficiently. This eliminates the need for joint training, significantly lowering both computational overhead and energy usage [38].

Other relevant details are outlined as follows. We use maximum diffusion timestep $T = 500$ and $0 \leq T' \leq T$. We set the learning rate varying from 1×10^{-3} to 1×10^{-4} . Adam optimizer was utilized for training, along with the ReduceLROnPlateau scheduler to dynamically adjust the learning rate, ensuring efficient convergence and preventing overfitting. Both MNIST and CIFAR-10 datasets are divided into two portions, with 60% allocated for the \mathcal{T} - \mathcal{R} pair and 40% designated for \mathcal{A}_a .

We reproduced several baseline models to provide a clear comparison and better evaluate the performance of our system.

- Information bottleneck theory and adversarial learning (named “IBAL”) [29], that could extract and transmit task-related features while enhancing privacy by significantly decreasing the SSIM and PSNR values of estimated images that the adversary could generate;
- IBAL under dynamic channel conditions (named “IBAL-D”) [29], that can adjust the weights of the classifier’s decision term and the attacker’s recovery term in the loss function based on the channel conditions.
- Direct mode (named “Direct”), where images $x \in X$ are directly distorted according to the channel conditions to get \ddot{x} , and then are classified by the strong classifier.
- Permutation mode (named “Permutation”) [31], where the order of elements of images are rearranged according to a specific permutation rule or key, without altering the actual content of the elements. Then permuted images are classified by the strong classifier.

B. Results on MNIST dataset

Fig. 4 provides a comprehensive performance comparison of various semantic communication systems for the MNIST dataset with a particular focus on accuracy, under channel SNR 15 dB. Here we provide another curve named “Classifier”, which means \hat{z} is directly sent into the classifier Θ_{θ} and bypasses the diffusion module. The green solid lines with notations stars and circles represent the classification accuracy of \hat{z} and \hat{x} , without other modules involved. They can be simply regarded as a classification task and an image restoration task under different channel conditions that are determined by t , and they reveal a fundamental gap that reflects the intrinsic difference between recovering task-specific features

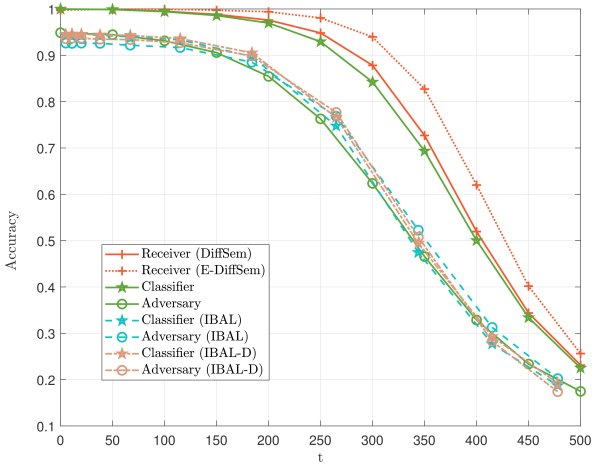


Fig. 4: System performances and baselines using MNIST dataset.

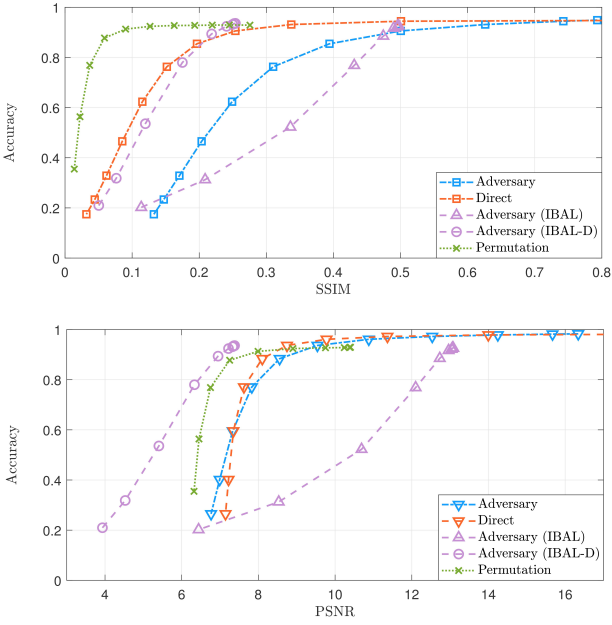


Fig. 5: Plot of accuracy versus SSIM and PSNR using MNIST dataset.

(task-oriented semantic information) and pixel-level details (syntactic information) given the specific task and dataset [8], confirming that task-oriented recovery is inherently more efficient. For example, at $t = 300$, the classifier achieves 84% accuracy, while the adversary's reconstructed images yield only 62% accuracy for the same task. Since semantic information is a highly condensed version of syntax and requires less feature to describe, reconstructing syntax is inherently more demanding than recovering semantics.

The two red lines at the top of the figure represent the classification accuracy of the receiver after incorporating the diffusion module. It can be observed that using DiffSem provides a slight improvement in the receiver's recovery, while the label-embedded E-DiffSem significantly enhances system performance. This aligns with the earlier discussion that $\sqrt{\alpha_t} f_0$ can be regarded as an intrinsic guide, and the

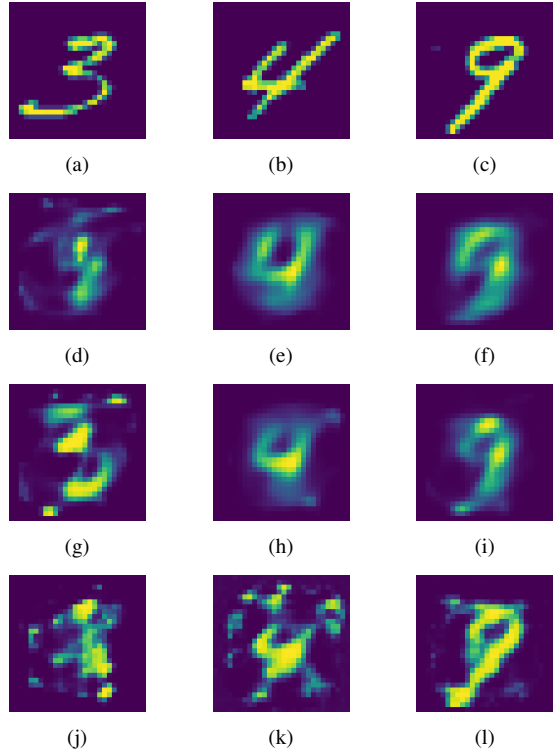


Fig. 6: Adversary's output images with different SNR or t under MNIST dataset. 1st row: -10 dB; $t = 344$. 2nd row: 0 dB; $t = 184$. 3rd row: 10 dB; $t = 67$. (a)(b)(c) Original images. (d)(e)(f) IBAL system. (g)(h)(i) IBAL-D system. (j)(k)(l) Our system.

receiver's preliminary recovery \hat{y} can serve as guidance to effectively boost diffusion. Most notably, when $t = 300$, DiffSem and E-DiffSem improve classification accuracy by 3.35% and 10.03% compared to the system without diffusion, respectively. One possible explanation for the superior performance of diffusion-aided methods lies in their ability to model complex distributions and generate high-quality reconstructions. Diffusion models iteratively refine the output by design, which aligns well with the requirements of semantic communication, where accurate reconstruction of semantic information is crucial. E-DiffSem further optimizes the diffusion process by effectively leveraging the label estimated by the classifier, leading to higher accuracy.

The IBAL and IBAL-D baselines provide an interesting contrast to the proposed methods. Note that the curves in Fig. 4 use SNR as the horizontal axis during training; here they have been recalculated based on Eq. (13) and presented with t as the horizontal axis. We employ the same strong classifier structure for all adversaries including the one in our system, ensuring a consistent ability to assess the amount of task-relevant information in reconstructed images. Since adversarial training, which is grounded in the information bottleneck principle, demands the careful navigation of a dynamic trade-off between the transmission of task-relevant information and the mitigation of adversarial threats, this inevitable compromise inherently limits the amount of information that can be transmitted during standard communication, ultimately causing a pronounced decline in the receiver's accuracy. In stark contrast, our diffusion-aided receiver demonstrates remarkable

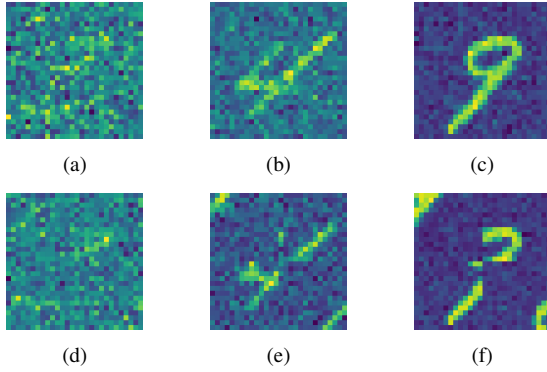


Fig. 7: (a)(b)(c) Direct mode and (d)(e)(f) permutation mode, with channel noise -10 dB, 0 dB, 10 dB. Original images are as (a)(b)(c) in Fig. 6.

superiority, achieving significantly higher performance compared to both IBAL systems.

Fig. 5 shows how accuracy varies with SSIM and PSNR on the MNIST dataset. Here, ‘‘Direct’’ and ‘‘Permutation’’ mean the accuracy of $\bar{\Theta}_\theta$ ’s classification to the original images and permuted images that are directly noised by a certain level of Gaussian white noise⁶ (as shown in Fig. 7), based on Eq. (11); we use a simple permutation method that divides the image into four parts and swaps the position of up-left corner and down-right corner parts. Essentially, our system’s adversary \mathcal{A}_a , as well as the adversaries in the two IBAL systems, can partially achieve the recovery of the input x , as evidenced by their SSIM values being higher than those of the direct-noising scenario in most cases with the same accuracy. This observation is consistent with neural-based systems that possess denoising capabilities [47]. Compared to the adversary in our system, despite the adversaries in both information-bottleneck-based systems effectively reduce the estimated SSIM and PSNR of the original input obtained by the attacker, we observe that there are cases that the adversary’s classification accuracy can remain relatively high. For example, when the SSIM is 0.2, the attacker in our system (blue dashed line) achieves a accuracy of 0.47, whereas IBAL-D (purple dashed line with circle markers) reaches 0.78 at SSIM = 0.175. This indicates that adversarial training merely distorts syntactic features without suppressing semantic information, since the key features remain intact or largely unchanged from the perspective of neural networks. It can be evidenced in Fig. 6 that the adversary’s images in IBAL still have enough semantic information that can be used to categorize, even though their SSIM or PSNR values are lower. The lower plot in Fig. 5, showing the complicated correspondence between PSNR and accuracy, further supports the discussion above, since PSNR ignores perceptual quality and structural information that is important to a classification task [32]. In task-oriented semantic communication, the primary goal is to accurately reconstruct and understand the transmitted task-related information, rather than merely preserving pixel-level

⁶Here we just use those two baselines as comparisons to show that SSIM or PSNR may be disconnected to the semantic fidelity in some cases, and the application of permutation is beyond our scope of this paper. Future work may utilize permutation to further enhance the system performance against model inversion attack.

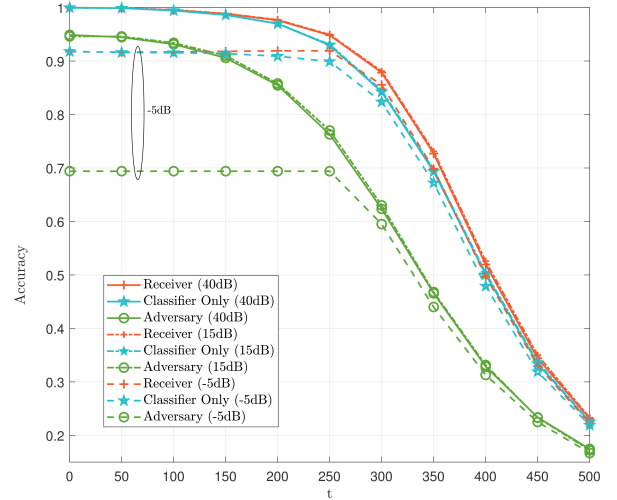


Fig. 8: System performances on MNIST dataset under AWGN channel with different channel SNRs.

fidelity. Therefore, metrics like accuracy, which directly measures the system’s ability to correctly interpret the semantic content, are more appropriate for evaluating the effectiveness of adversarial attacks.

The training strategy of our system prioritizes the recovery of semantic information. The adversary is only tasked with reconstructing images after the $\mathcal{T} - \mathcal{R}$ pair is fully trained to recover task-relevant semantic information, and the amount of information in \mathcal{T} ’s output can be considered constant. Since we further process the adversary’s output through a strong classifier that effectively converting the image reconstruction task into a classification task, it allows us to evaluate how much of the ‘‘task-relevant’’ information is contained within the reconstructed images, which is directly tied to the quality of the image reconstruction. However, due to the limited information provided by \mathcal{T} and the fact that the \mathcal{T} ’s output is not primarily designed for image reconstruction, the adversary’s ability to recover syntactic information is inherently biased, resulting in less ‘‘task-relevant’’ information embedded in the reconstructed images. If the $\mathcal{T} - \mathcal{A}$ pair is trained first, followed by the receiver \mathcal{R} , the training process would inevitably prioritize a ‘‘high-information task’’ (image reconstruction) before transitioning into a ‘‘low-information task’’ (classification). This approach would likely lead to the encoder producing excessive information, which would benefit the adversary by providing more access to task-relevant semantic information, even if the recovered images have relatively low SSIM (or PSNR) values. Consequently, this strategy would compromise the privacy protection intended for the classifier.

Fig. 8 illustrates the robustness of our DiffSem system across diverse channel conditions. As outlined in Sec. III Part C, the transmitter dynamically adjusts the level of self-noising pre-added noise based on the estimated channel condition. When facing high SNR regimes, the self-noising module becomes the primary driver of signal distortion, meaning that variations in t more directly influence the performance of both the receiver and the attacker, allowing precise control via t .

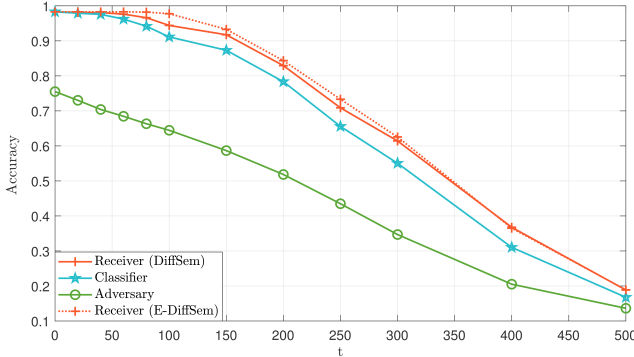


Fig. 9: System performances using CIFAR-10 dataset.

Conversely, in poor channel conditions, the wireless channel itself dominates, allowing the self-noising module to flexibly control the quality of the transmitted signal while preventing over-compression to exert minimal impact on the signal state at the receiver. For instance, at a channel SNR of -5 dB, the dominance of channel noise results in a nearly constant information gap between the classifier and the adversary. We observe that for $t > 250$, the performance of both the receiver and the adversary slightly deteriorates compared to scenarios with higher channel SNR. This discrepancy may stem from the discrete nature of $\bar{\alpha}_t$, causing deviations between practical estimates and theoretical calculations. Overall, our self-noising module effectively modulates the degree of signal distortion in response to wireless channel conditions, maintaining an appropriate noise margin and ensuring reliable operation under both high and low SNR environments.

C. Results on CIFAR-10 dataset

We also implement the system on the CIFAR-10 dataset, which has complex scenes that pose more challenges for semantic communication systems. Fig. 9 illustrates the receiver's classification accuracy and the attacker's success rate as functions of t . Given our assumption that the training of the $\mathcal{T} - \mathcal{R}$ pair takes precedence over the adversary's training, even at $t = 0$, the classification accuracy of the adversary's reconstructed images is not very high. This is because the $\mathcal{T} - \mathcal{R}$ pair's training prioritizes the completion of the label classification task, and the backpropagation process optimizes the \mathcal{T} 's neural network in a way that is not aligned with the adversary's image recovery requirements, which is acceptable since normal systems are not designed to meet attackers' needs.

The two red lines in Fig. 9 show that the system incorporating the diffusion module outperforms the classifier-only scenario. This indicates that imperfect labels can still provide coarse-grained constraints for the diffusion path. However, the additional performance improvement brought by E-DiffSem is less pronounced compared to the MNIST dataset. This discrepancy may be because the CIFAR-10 dataset contains richer and more complex information than MNIST, which makes it more challenging for the imperfect labels estimated by the classifier to provide effective guidance to the diffusion module. In the future, we could explore integrating Transformer-based self-attention mechanisms or leveraging

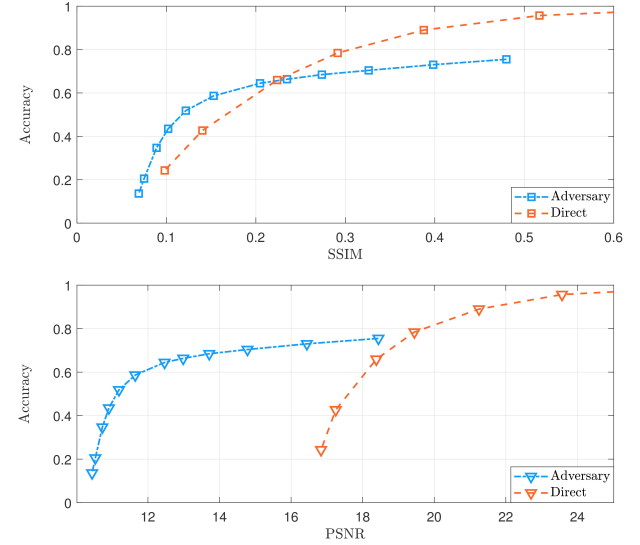


Fig. 10: Plot of accuracy versus SSIM and PSNR using CIFAR-10 dataset.

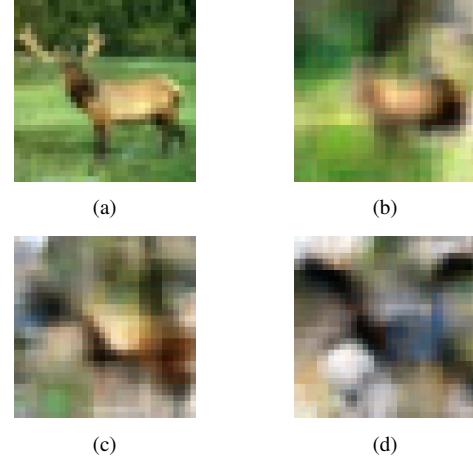


Fig. 11: Adversary's output images with different t under CIFAR-10 dataset. (a) Original image. (b)(c)(d) Adversary's recovery when $t = 60, 150$ and 300 .

image semantic segmentation techniques to provide stronger guidance for the diffusion module, thereby further enhancing system performance.

As shown in Fig. 11, our system actively degrades the semantic utility of adversarial reconstructions. For instance, at $t = 150$ ($p = 2.3$ dB), the adversary's recovered images (Fig. 11(c)) retain only fragmented visual cues (e.g., partial textures), resulting in a classification accuracy of 58.7%, which is significantly below 87.3% when bypassing diffusion, as well as 91.7% and 93.3% when using DiffSem and E-DiffSem. The gaps stem from our diffusion model's prioritized recovery of task-specific features (e.g., object categories) while discarding non-essential syntactic details. Such a design ensures that even if attackers partially reconstruct pixel-level content, they cannot infer semantic information effectively in a certain possibility.

Fig. 10 shows the accuracy versus SSIM and PSNR on the CIFAR-10 dataset. It highlights the weak correlation between

traditional image quality metrics and semantic security. For instance, when SSIM is 0.12, the attacker's classification accuracy still reaches 51.8%, whereas in the direct mode, with SSIM equal to 0.14, the accuracy is only 42.6%. This difference arises from the attacker's ability to implicitly learn class-discriminative features, while variations in pixel texture are insufficient to prevent the attacker from acquiring these features. Other curves in this figure can further demonstrate that SSIM and PSNR are not suitable metrics for evaluating the amount of task-relevant information obtained by the attacker in task-oriented communication systems.

As a supplement to the discussion, we comment on the computational complexity of our proposed system. Our hardware conditions are: CPU, Intel Xeon Gold 5220; GPU, GeForce RTX 3090. Although the diffusion model introduces additional computational overhead, the DDIM acceleration strategy restricts the additional single-sample inference time of DiffSem to approximately 0.1s per batch (batch size 256) on CIFAR-10. It shows that the performance enhancement does not impose a substantial computational burden given the relatively small dataset. For higher-resolution datasets, such as ImageNet, the trade-off between performance improvement and computational cost may become a critical consideration, especially in real-time applications where latency is a key factor. Future work could focus on optimizing the diffusion process, potentially exploring techniques such as knowledge distillation, model pruning, or adopting more efficient neural network architectures to address this challenge.

V. CONCLUSION

In this paper, we introduce DiffSem, a diffusion-aided framework for task-oriented semantic communication, designed to balance task performance and privacy preservation. We generalize the algorithm by defining the success rate of model inversion via the attacker's task accuracy, rather than pixel-level similarity metrics. DiffSem instantiates a non-adversarial privacy preserving mechanism that exploits the inherent mismatch between the task-specific semantics required by the legitimate receiver and the broader context that the attacker must reconstruct. Specifically, a transmitter-side self-noise mechanism adaptively regulates the radiated semantic information while compensating for channel noise, an unguided diffusion U-Net on the receiver enhances performance on downstream tasks, and an optional self-referenced label embedding further enhances receiver performance while maintaining the guidance-free constraint. Experiments show that DiffSem enables the legitimate receiver to achieve higher accuracy than the baseline, and highlight the potential mismatch between traditional image quality metrics and task-oriented semantic fidelity. Overall, DiffSem provides a unified and non-adversarial approach to balance utility and privacy in semantic communication, while our attacker accuracy-based evaluation method provides a more appropriate perspective for evaluating and mitigating model reversal risks in practice.

APPENDIX A DERIVATION OF EQ. (24)

Here we derive the Eq. (24) in detail. Since we have

$$\mathbb{E}(\|z'\|^2) = \bar{\alpha}_{T'} \|f_0\|^2 + (1 - \bar{\alpha}_{T'}) D \quad (25)$$

and

$$\begin{aligned} \mathbb{E}(\|\hat{z}''\|^2) &= \bar{\alpha}_{T'} \|f_0\|^2 + (1 - \bar{\alpha}_{T''}) D + \sigma_{\text{ch}}^2 D \\ &= \bar{\alpha}_{T'} \|f_0\|^2 + (1 - \bar{\alpha}_{T''}) D \\ &\quad + \frac{\bar{\alpha}_{T'} \mathbb{E}(\|f_0\|^2) + (1 - \bar{\alpha}_{T''}) D}{\gamma} D, \end{aligned} \quad (26)$$

we can get

$$1 - \bar{\alpha}_{T''} + \frac{\bar{\alpha}_{T'} \mathbb{E}(\|f_0\|^2) + (1 - \bar{\alpha}_{T''}) D}{\gamma} = 1 - \bar{\alpha}_{T'} \quad (27)$$

when $\mathbb{E}(\|z'\|^2) = \mathbb{E}(\|\hat{z}''\|^2)$. Then

$$\bar{\alpha}_{T''} \left(1 + \frac{D}{\gamma} \right) = \bar{\alpha}_{T'} \left(1 + \frac{\mathbb{E}(\|f_0\|^2)}{\gamma} \right) + \frac{D}{\gamma}. \quad (28)$$

Arranging the formula above, we can get

$$\bar{\alpha}_{T''} = \frac{\bar{\alpha}_{T'} (\gamma + \mathbb{E}(\|f_0\|^2)) + D}{\gamma + D}. \quad (29)$$

REFERENCES

- [1] W. Weaver, "Recent contributions to the mathematical theory of communication," *ETC: a review of general semantics*, pp. 261–281, 1953.
- [2] Y. Shao, Q. Cao, and D. Gündüz, "A theory of semantic communication," *IEEE Transactions on Mobile Computing*, 2024.
- [3] H. Pan, S. Yang, T.-T. Chan, Z. Wang, V. C. Leung, and J. Li, "SC-PNC: Semantic communication-empowered physical-layer network coding," *IEEE Transactions on Cognitive Communications and Networking*, vol. 10, no. 4, pp. 1160–1174, 2024.
- [4] H. Xie, Z. Qin, G. Y. Li, and B.-H. Juang, "Deep learning enabled semantic communication systems," *IEEE transactions on signal processing*, vol. 69, pp. 2663–2675, 2021.
- [5] E. Beck, C. Bockelmann, and A. Dekorsy, "Semantic communication: An information bottleneck view," *arXiv preprint arXiv:2204.13366*, 2022.
- [6] L. Yan, Z. Qin, R. Zhang, Y. Li, and G. Y. Li, "Resource allocation for text semantic communications," *IEEE Wireless Communications Letters*, vol. 11, no. 7, pp. 1394–1398, 2022.
- [7] X. Peng, Z. Qin, X. Tao, J. Lu, and L. Hanzo, "A robust semantic text communication system," *IEEE Transactions on Wireless Communications*, 2024.
- [8] Z. Lyu, G. Zhu, J. Xu, B. Ai, and S. Cui, "Semantic communications for image recovery and classification via deep joint source and channel coding," *IEEE Transactions on Wireless Communications*, vol. 23, no. 8, pp. 8388–8404, 2024.
- [9] H. Wu, Y. Shao, C. Bian, K. Mikolajczyk, and D. Gündüz, "Deep joint source-channel coding for adaptive image transmission over MIMO channels," *IEEE Transactions on Wireless Communications*, 2024.
- [10] Q. Ma, J. Pan, and C. Bai, "Direction-oriented visual-semantic embedding model for remote sensing image-text retrieval," *IEEE Transactions on Geoscience and Remote Sensing*, 2024.
- [11] H. Li, H. Tong, S. Wang, N. Yang, Z. Yang, and C. Yin, "Video semantic communication with major object extraction and contextual video encoding," in *2024 IEEE Wireless Communications and Networking Conference (WCNC)*. IEEE, 2024, pp. 1–6.
- [12] S. Wang, J. Dai, Z. Liang, K. Niu, Z. Si, C. Dong, X. Qin, and P. Zhang, "Wireless deep video semantic transmission," *IEEE Journal on Selected Areas in Communications*, vol. 41, no. 1, pp. 214–229, 2022.
- [13] Y. Cang, M. Chen, Z. Yang, Y. Hu, Y. Wang, C. Huang, and Z. Zhang, "Online resource allocation for semantic-aware edge computing systems," *IEEE Internet of Things Journal*, vol. 11, no. 17, pp. 28094–28110, 2023.

[14] W. Yang, Z. Q. Liew, W. Y. B. Lim, Z. Xiong, D. Niyato, X. Chi, X. Cao, and K. B. Letaief, "Semantic communication meets edge intelligence," *IEEE wireless communications*, vol. 29, no. 5, pp. 28–35, 2022.

[15] K. Muhammad, T. Hussain, H. Ullah, J. Del Ser, M. Rezaei, N. Kumar, M. Hijji, P. Bellavista, and V. H. C. de Albuquerque, "Vision-based semantic segmentation in scene understanding for autonomous driving: Recent achievements, challenges, and outlooks," *IEEE Transactions on Intelligent Transportation Systems*, vol. 23, no. 12, pp. 22 694–22 715, 2022.

[16] G. Zheng, Q. Ni, K. Navaie, H. Pervaiz, and C. Zarakovitis, "A distributed learning architecture for semantic communication in autonomous driving networks for task offloading," *IEEE Communications Magazine*, vol. 61, no. 11, pp. 64–68, 2023.

[17] H. Zhang, H. Wang, Y. Li, K. Long, and V. C. Leung, "Toward intelligent resource allocation on task-oriented semantic communication," *IEEE Wireless Communications*, vol. 30, no. 3, pp. 70–77, 2023.

[18] D. Gündüz, Z. Qin, I. E. Aguerri, H. S. Dhillon, Z. Yang, A. Yener, K. K. Wong, and C.-B. Chae, "Beyond transmitting bits: Context, semantics, and task-oriented communications," *IEEE Journal on Selected Areas in Communications*, vol. 41, no. 1, pp. 5–41, 2022.

[19] M. Jankowski, D. Gündüz, and K. Mikolajczyk, "Deep joint source-channel coding for wireless image retrieval," in *ICASSP 2020-2020 IEEE International Conference on Acoustics, Speech and Signal Processing (ICASSP)*. IEEE, 2020, pp. 5070–5074.

[20] H. Sun, W. Ni, H. Tian, J. Zheng, G. Nie, and D. Niyato, "A Hybrid Federated Learning Framework for Task-Oriented Semantic Communication," *IEEE Internet of Things Journal*, 2025.

[21] J. Peng, H. Xing, Y. Li, L. Feng, L. Xu, and X. Lei, "Task-oriented multi-user semantic communication with lightweight semantic encoder and fast training for resource-constrained terminal devices," *IEEE Wireless Communications Letters*, 2024.

[22] C. Cai, X. Yuan, and Y.-J. A. Zhang, "End-to-End Learning for Task-Oriented Semantic Communications Over MIMO Channels: An Information-Theoretic Framework," *IEEE Journal on Selected Areas in Communications*, 2025.

[23] Z. Yang, M. Chen, G. Li, Y. Yang, and Z. Zhang, "Secure semantic communications: Fundamentals and challenges," *IEEE network*, 2024.

[24] T. Ha, T. K. Dang, T. T. Dang, T. A. Truong, and M. T. Nguyen, "Differential privacy in deep learning: an overview," in *2019 International Conference on Advanced Computing and Applications (ACOMP)*. IEEE, 2019, pp. 97–102.

[25] K. Pan, Y.-S. Ong, M. Gong, H. Li, A. K. Qin, and Y. Gao, "Differential privacy in deep learning: A literature survey," *Neurocomputing*, p. 127663, 2024.

[26] L. Zhao, D. Wu, and L. Zhou, "Data utilization versus privacy protection in semantic communications," *IEEE Wireless Communications*, vol. 30, no. 3, pp. 44–50, 2023.

[27] T. Xiao, Y.-H. Tsai, K. Sohn, M. Chandraker, and M.-H. Yang, "Adversarial learning of privacy-preserving and task-oriented representations," in *Proceedings of the AAAI Conference on Artificial Intelligence*, vol. 34, no. 07, 2020, pp. 12 434–12 441.

[28] A. Li, Y. Duan, H. Yang, Y. Chen, and J. Yang, "TIPRDC: task-independent privacy-respecting data crowdsourcing framework for deep learning with anonymized intermediate representations," in *Proceedings of the 26th ACM SIGKDD international conference on knowledge discovery & data mining*, 2020, pp. 824–832.

[29] Y. Wang, S. Guo, Y. Deng, H. Zhang, and Y. Fang, "Privacy-preserving task-oriented semantic communications against model inversion attacks," *IEEE Transactions on Wireless Communications*, 2024.

[30] G. Shi, D. Gao, X. Song, J. Chai, M. Yang, X. Xie, L. Li, and X. Li, "A new communication paradigm: From bit accuracy to semantic fidelity," *arXiv preprint arXiv:2101.12649*, 2021.

[31] Y. Chen, Q. Yang, Z. Shi, and J. Chen, "The model inversion eavesdropping attack in semantic communication systems," in *GLOBECOM 2023-2023 IEEE Global Communications Conference*. IEEE, 2023, pp. 5171–5177.

[32] Z. Wang, A. C. Bovik, H. R. Sheikh, and E. P. Simoncelli, "Image quality assessment: from error visibility to structural similarity," *IEEE transactions on image processing*, vol. 13, no. 4, pp. 600–612, 2004.

[33] F.-A. Croitoru, V. Hondru, R. T. Ionescu, and M. Shah, "Diffusion models in vision: A survey," *IEEE Transactions on Pattern Analysis and Machine Intelligence*, vol. 45, no. 9, pp. 10 850–10 869, 2023.

[34] L. Yang, Z. Zhang, Y. Song, S. Hong, R. Xu, Y. Zhao, W. Zhang, B. Cui, and M.-H. Yang, "Diffusion models: A comprehensive survey of methods and applications," *ACM Computing Surveys*, vol. 56, no. 4, pp. 1–39, 2023.

[35] E. Grassucci, C. Marinoni, A. Rodriguez, and D. Comminiello, "Diffusion models for audio semantic communication," in *ICASSP 2024-2024 IEEE International Conference on Acoustics, Speech and Signal Processing (ICASSP)*. IEEE, 2024, pp. 13 136–13 140.

[36] T. Wu, Z. Chen, D. He, L. Qian, Y. Xu, M. Tao, and W. Zhang, "CDDM: Channel denoising diffusion models for wireless semantic communications," *IEEE Transactions on Wireless Communications*, 2024.

[37] L. Guo, W. Chen, Y. Sun, B. Ai, N. Pappas, and T. Quek, "Diffusion-driven semantic communication for generative models with bandwidth constraints," *IEEE Transactions on Wireless Communications*, 2025.

[38] E. Grassucci, S. Barbarossa, and D. Comminiello, "Generative semantic communication: Diffusion models beyond bit recovery," *arXiv preprint arXiv:2306.04321*, 2023.

[39] O. Erak, O. Alhussein, and W. Tong, "Contrastive Learning and Adversarial Disentanglement for Task-Oriented Semantic Communications," *arXiv preprint arXiv:2410.22784*, 2024.

[40] U. Schilcher, C. Bettstetter, and G. Brandner, "Temporal correlation of interference in wireless networks with Rayleigh block fading," *IEEE Transactions on Mobile Computing*, vol. 11, no. 12, pp. 2109–2120, 2011.

[41] D. Tse and P. Viswanath, *Fundamentals of wireless communication*. Cambridge university press, 2005.

[42] A. Goldsmith, *Wireless communications*. Cambridge university press, 2005.

[43] Z. Gu, H. Jamjoom, D. Su, H. Huang, J. Zhang, T. Ma, D. Pendarakis, and I. Molloy, "Reaching data confidentiality and model accountability on the caltrain," in *2019 49th Annual IEEE/IFIP International Conference on Dependable Systems and Networks (DSN)*. IEEE, 2019, pp. 336–348.

[44] M. Fredrikson, S. Jha, and T. Ristenpart, "Model inversion attacks that exploit confidence information and basic countermeasures," in *Proceedings of the 22nd ACM SIGSAC conference on computer and communications security*, 2015, pp. 1322–1333.

[45] H. Fang, Y. Qiu, H. Yu, W. Yu, J. Kong, B. Chong, B. Chen, X. Wang, S.-T. Xia, and K. Xu, "Privacy leakage on DNNs: A survey of model inversion attacks and defenses," *arXiv preprint arXiv:2402.04013*, 2024.

[46] J. Song, C. Meng, and S. Ermon, "Denoising diffusion implicit models," *arXiv preprint arXiv:2010.02502*, 2020.

[47] X. Wang and L. Lu, "Implementation of DNN-based physical-layer network coding," *IEEE Transactions on Vehicular Technology*, vol. 72, no. 6, pp. 7380–7394, 2023.